Caldeira-Leggett model versus ab initio potential: A vibrational spectroscopy test of water solvation

Alessandro Rognoni, Riccardo Conte, and Michele Ceotto*

Dipartimento di Chimica, Università degli Studi di Milano, via Golgi 19, 20133 Milano, Italy

Abstract

We present a semiclassically approximate quantum treatment of solvation with the purpose of investigating the accuracy of the Caldeira-Leggett model. We do that by simulating the vibrational features of water solvation by means of two different approaches. One is entirely based on the adoption of an accurate ab initio potential to describe water clusters of increasing dimensionality. The other one consists of a model made of a central water molecule coupled to a high-dimensional Caldeira-Leggett harmonic bath. We demonstrate the role of quantum effects in the detection of water solvation and show that the computationally cheap approach based on the Caldeira-Leggett bath is only partially effective. The main conclusion of the study is that quantum methods associated to high-level potential energy surfaces are necessary to correctly study solvation features, while simplified models, even if attractive owing to their reduced computational cost, can provide some useful insights but are not able to come up with a comprehensive description of the solvation phenomenon.

* michele.ceotto@unimi.it

I. INTRODUCTION

The comprehension of condensed-phase processes is one of the main challenges in chemistry because of their intrinsic complexity. They involve the interaction of a system with the environment, which is difficult to investigate due to the high number of degrees of freedom in play. However, constant research is necessary since condensed-phase chemistry is ubiquitous and of utmost importance for the description of natural processes. For instance, liquid water and aqueous systems are at the heart of life and they have been the subject of countless studies. In this field, key phenomena like protein folding and biological reactions in condensed phase are just a couple of remarkable examples. It is not surprising that much research effort is being made to reach a detailed and accurate description of these processes. In particular, vibrational spectroscopies have emerged as powerful techniques to study the solvation mechanisms and a primary tool to elucidate hydrogen bond structure and dynamics.[1–4] By combining spectroscopic theory and experiments, it is now possible to gain deeper understanding on the many open issues in the field of solvation.

By far, the most studied and interesting solvent is water and huge progress in the description of water under all physical states has been recently made. However, the great number of degrees of freedom (DOFs) involved, the well-known floppiness of aqueous systems, and the high level of theory often required to obtain quantitative results end up making the study of solvated systems a formidably difficult task. Nevertheless, theoretical methods able to recover quantum mechanical effects are often necessary to properly compare simulations with experimental results. This is because quantum effects can indeed play an important role in determining the static and dynamical properties of water.[5–8]

From the theoretical point of view, these issues require highly accurate simulations and prompted the construction of ab initio potential energy surfaces (PESs) to study water and solvated systems.[9–12]These potentials are obtained by fitting high-level coupled-cluster data and provide highly accurate energies yet at a convenient computational cost.[13–15] However, for very high-dimensional solvated systems ab initio potentials can be way too computationally demanding. In those cases, simplified and model potentials can be employed to greatly reduce the computational cost.[16–19] Among them, the Caldeira-Leggett model has gained popularity in the study of condensed-phase systems, even spectroscopically.[20–25]

The Caldeira-Leggett model is certainly a very useful theoretical tool, allowing for physical interpretation and identification of the key properties of a system starting from just a few parame-

ters. However, in a spectroscopic context its ability to describe anharmonic spectra of real systems should not be taken for granted.[26] A possible way to measure the accuracy of the Caldeira-Leggett model is by calculating the vibrational energy eigenvalues, i.e. what is called the quantum power spectrum. Specifically, if one is able to compare the quantum eigenvalues obtained from the model potential with those calculated employing highly accurate PESs and with experimental Infrared (IR) transitions, then it is possible to assess the quality of the model potential in the description of the system of interest. To this end, it is crucial to have a quantum mechanical approach available that is able to deal with high-dimensional systems. Moreover, it is also important that in a system-bath study one performs a correct assignment of the spectroscopic signals by being able to isolate those ones originated by the system from the plethora of fundamentals, overtones, and combination bands associated to the bath DOFs.

In the context of vibrational spectroscopy, Semiclassical Initial Value Representation (SCIVR) molecular dynamics[27–42] is a valuable tool for the calculation of quantum vibrational energy levels.[43–46] The method is not affected by the notorious classical trajectory Zero Point Energy leakage issue,[47] and among all the possible simulation approaches, the Multiple-Coherent Divide-and-Conquer Semiclassical Initial Value Representation (MC-DC SCIVR) method has emerged as a powerful technique to compute vibrational spectra and eigenfunctions.[48–53] The underlying idea is to project the full-dimensional system onto lower-dimensional subspaces and to calculate the reduced-dimensionality spectra employing just a handful of classical trajectories. Then, the total spectrum is obtained by collecting all the lower-dimensional ones. This machinery allows one to retrieve clear spectroscopic signals even for high-dimensional and complex systems. Over the past years, MC-DC SCIVR has been applied to the study of systems like small peptides and organic molecules,[54, 55] glycine supramolecular systems,[56], nucleobases and nucleotides,[57, 58] and molecules adsorbed on titania surfaces.[59] Furthermore, MC-DC SCIVR is being adopted to answer the question concerning the minimum number of water molecules necessary to fully solvate one.[60]

In this work, we first confirm the applicability of MC-DC SCIVR to very high dimensional systems. This is done by investigating water clusters of increasing dimensionality up to the solvation regime using an ab initio potential and by computing the vibrational spectra of several Caldeira-Leggett models of increasing complexity for different parameter choices. Then, to best assess the importance of an accurate description of the potential energy surface, we consider a model consisting of a water molecule coupled to a high-dimensional Caldeira-Leggett potential,

and compare the results with the IR spectrum of liquid water and with semiclassical simulations of water clusters. Furthermore, in an effort to point out the importance of quantum effects even in solvated systems, the quantum dynamical calculations in semiclassical approximation are also compared to quasi-classical simulations. A final analysis allows us to point out the necessity of performing quantum calculations associated to a very accurate description of the ab initio potential energy landscape in order to achieve a correct and complete description of water solvation.

The manuscript is organized as follows: After reviewing in Sec. II the basic theory of semiclassical and quasiclassical spectra, we perform spectroscopy calculations on several water clusters and solvated systems by means of both MC-DC SCIVR and the quasi-classical approach using the pre-existing MB-pol PES and the Caldeira-Leggett model potential. They are presented in Sec. III, which is ended by a detailed comparison between Caldeira-Leggett and ab initio results. Finally, Sec. IV recaps our results and concludes the manuscript.

II. THEORETICAL DETAILS

A. Semiclassical vibrational spectroscopy

The key point of this work is the determination of vibrational spectra. Following a time-dependent approach, the vibrational power spectrum $I(E)$ can be computed by Fourier transforming the wavepacket survival amplitude[61]

$$I(E) = \frac{1}{2\pi} \int_{-\infty}^{+\infty} dt\, e^{iEt} \langle \chi | \chi(t) \rangle, \tag{1}$$

in which $I(E)$ is the vibrational density of states at energy E, t is the time, $|\chi\rangle$ is an arbitrary quantum reference state and $\hbar$ has been set equal to 1. By writing the reference state as a linear combination of the Hamiltonian eigenfunctions, $|\chi\rangle = \sum_n c_n |\psi_n\rangle$, one can show that the previous equation is equal to a sum of delta functions centered at the vibrational energy levels

$$I(E) = \sum_n |c_n|^2 \delta(E - E_n). \tag{2}$$

Within the semiclassical framework, a convenient way to calculate $I(E)$ is the one developed by Kaledin and Miller, where the spectral density is reproduced using a time-averaged semiclassical

Initial Value Representation (TA SCIVR) method.[43, 44] For an F-dimensional system, the TA-SCIVR expression in the separable approximation is

$$I(E) = \frac{1}{(2\pi)^F} \iint d\boldsymbol{p}_0 d\boldsymbol{q}_0 \frac{1}{2\pi T} \left| \int_0^T dt \, \langle \chi | \boldsymbol{p}_t, \boldsymbol{q}_t \rangle \, e^{i(S_t(\boldsymbol{p}_0,\boldsymbol{q}_0)+\phi_t(\boldsymbol{p}_0,\boldsymbol{q}_0)+Et)} \right|^2 , \tag{3}$$

where $\boldsymbol{p}_0$ and $\boldsymbol{q}_0$ are the initial momenta and positions, T is the total simulation time, $S_t(\boldsymbol{p}_0, \boldsymbol{q}_0)$ is the classical action, and $|\boldsymbol{p}_t \boldsymbol{q}_t\rangle$ are coherent states of the type

$$\langle \boldsymbol{x} | \boldsymbol{p}, \boldsymbol{q} \rangle = \left(\frac{\det(\boldsymbol{\gamma})}{\pi^F} \right)^{\frac{1}{4}} \exp \left[-\frac{1}{2} (\boldsymbol{x} - \boldsymbol{q})^{\mathrm{T}} \boldsymbol{\gamma} (\boldsymbol{x} - \boldsymbol{q}) + i \boldsymbol{p}^{\mathrm{T}} (\boldsymbol{x} - \boldsymbol{q}) \right] . \tag{4}$$

In this equation $\boldsymbol{\gamma}$ is a diagonal matrix whose elements are chosen to be numerically equal to the harmonic frequencies of the vibrational normal modes. Mass-scaled coordinates have been introduced to simplify the notation. In Eq. (3), $\phi(\boldsymbol{p}_0, \boldsymbol{q}_0)$ is the phase of the Herman-Kluk prefactor.[30, 62–65] The major problem associated to the TA-SCIVR formula is the so-called "curse of dimensionality". If the system is composed of too many degrees of freedom (DOFs), the overlap integral in Eq. (1) is too difficult to converge, ending up in producing a noisy or even a signal-missing spectrum, as we will show below. To overcome this problem, the Divide-and-Conquer (DC) SCIVR has been recently introduced.[48, 66] The basic principle is to project all the quantities appearing in the previous equation onto lower-dimensional subspaces. In this way, it is possible to calculate reduced-dimensionality spectra. Eventually, the complete spectrum is simply obtained by collecting all the low-dimensional ones. The DC-SCIVR working equation is

$$\tilde{I}(E) = \frac{1}{(2\pi)^N} \iint d\tilde{\boldsymbol{p}}_0 d\tilde{\boldsymbol{q}}_0 \frac{1}{2\pi T} \left| \int_0^T dt \, \langle \tilde{\chi} | \tilde{\boldsymbol{p}}_t, \tilde{\boldsymbol{q}}_t \rangle \, e^{i\left(\tilde{S}_t(\boldsymbol{p}_0,\boldsymbol{q}_0)+\tilde{\phi}_t(\boldsymbol{p}_0,\boldsymbol{q}_0)+Et\right)} \right|^2 , \tag{5}$$

in which the quantities projected onto an N-dimensional subspace are indicated with the tilde (~) symbol. All the terms appearing in Eq. (5) can be straightforwardly projected except for the action, because the potential $V(\boldsymbol{q})$ is generally not separable (*i.e.* it cannot be written down exactly as a sum of terms originating from the different subspaces). To project the action we adopted the following equation:

$$\tilde{S}_t(\boldsymbol{p}_0, \boldsymbol{q}_0) = \int_0^t dt' \left[\frac{1}{2} \tilde{\boldsymbol{p}}_{t'}{}^T \tilde{\boldsymbol{p}}_{t'} - \left(V(\tilde{\boldsymbol{q}}_{t'}, \boldsymbol{q}_{t'}^{(F-N)}) - V(\tilde{\boldsymbol{q}}_{eq}, \boldsymbol{q}_{t'}^{(F-N)}) \right) \right] , \tag{6}$$

which is exact for separable potentials and approximates the correct projected action for non-separable ones. DC SCIVR has already been applied to systems as big as the fullerene molecule and to complex and fluxional molecules like the protonated water dimer and small water clusters.[48, 49, 67] For very high dimensional systems, a converged integration over the phase space of Eq. (5) can be too computationally demanding to be calculated. For this reason, we developed and applied the multiple-coherent states DC-SCIVR (MC-DC SCIVR) approach. The idea is to replace the double integral with a sum over the most relevant trajectories for the spectrum. Those trajectories are the ones having energy as close as possible to the quantum mechanical eigenvalue.[68] An educated guess for the initial conditions is to set the positions equal to the equilibrium ones, while adopting a harmonic estimate for the momenta. For the generic jth degree of freedom these are[69]

$$\begin{cases} q_0^{(j)} = q_{eq}^{(j)} \\ p_0^{(j)} = \sqrt{(2n_j+1)\omega_j} \end{cases} , \tag{7}$$

where $q_{eq}^{(j)}$ is the equilibrium position of the jth degree of freedom, ω_j its harmonic frequency and n_j the vibrational quantum number. The reference state is composed of linearly-combined coherent states:

$$|\tilde{\chi}\rangle = \prod_i^N \left(|p_0^{(i)}, q_0^{(i)}\rangle + \epsilon_i | - p_0^{(i)}, q_0^{(i)}\rangle \right), \tag{8}$$

where the product runs over all the modes belonging to the N-dimensional subspace. ϵ_i are coefficients selected to enhance the signals coming from different normal modes according to their symmetry. When their values is a collection of $+1$, all the intensities of the spectroscopic peaks associated to even vibrational quantum numbers (including the Zero Point Energy one) are amplified, while signals corresponding to odd values of the quantum number of the ith mode are selected by setting $\epsilon_i = -1$.[70] The MC-DC-SCIVR approach allowed the study of high-dimensional systems like glycine supramolecular systems, dipeptide derivatives, and nucleobases.[54, 56, 57]

We then label MC SCIVR the method for which we applied the MC idea to Eq. (3), thus obtaining a level of approximation higher than the TA-SCIVR formula but lower than MC-DC SCIVR for non-separable systems. However, the lack of a projection procedure causes the convergence problems already mentioned for TA SCIVR, if the dimensionality of the system is too high. This

method has been applied to the study of systems like ammonia, for which MC SCIVR was able to capture the deep tunneling splittings associated to the inversion of the umbrella motion, and to the glycine amino acid.[71, 72].

In all semiclassical propagations, the computational bottleneck is given by the calculation of $\tilde{\phi}_t(\boldsymbol{p}_0, \boldsymbol{q}_0)$, because its time propagation requires the evaluation of the full-dimensional Hessian matrices 4 times for each time-step, if a fourth order symplectic integrator is employed.[73] To reduce the computational cost, we adopted the approximation $\tilde{\phi}(\boldsymbol{p}, \boldsymbol{q}) \approx \phi(\tilde{\boldsymbol{p}}, \tilde{\boldsymbol{q}})$. Instead of projecting the full-dimensional prefactor, which would require the evaluation of full-dimensional Hessians, we built the phase directly within each subspace. This procedure allows us to calculate only reduced-dimensionality Hessians and save computational time. This approximation has been already applied to the study of molecules adsorbed on TiO_2 surfaces demonstrating its accuracy.[59]

B. The Quasiclassical approach

In addition to semiclassical simulations, we also computed quasiclassical spectra.[56, 67] Quasiclassical simulations turned out to be useful to identify peaks coming from bath degrees of freedom in Caldeira-Leggett spectra, and to point out the presence of nuclear quantum effects in water clusters simulations. In a quasiclassical simulation, we evolve a single trajectory with initial conditions as given in Eq. (7). Then, the Fourier transform of the velocity-velocity correlation function is computed along the path to calculate the quasiclassical power spectrum. Using mass-scaled coordinates and considering a one-dimensional problem for simplicity (although it can be straightforwardly generalized to multidimensional systems), the velocity-velocity correlation function is equal to:[74]

$$G(\tau) = \langle p(t)p(t+\tau)\rangle = \frac{1}{T}\int_0^T dt\, p(t)p(t+\tau), \tag{9}$$

where a sufficiently long total simulation time is assumed. The spectrum is then computed from the Fourier transform of $G(\tau)$:

$$I(\omega) = \int_{-\infty}^{+\infty} d\tau\, e^{i\omega\tau} G(\tau). \tag{10}$$

Inserting Eq. (9) into Eq. (10), writing $p(t)$ and $p(t+\tau)$ as inverse Fourier transforms of $\tilde{p}(\omega')$ and $\tilde{p}(\omega'')$, and rearranging the integrals, one obtains:

$$I(\omega) = \frac{1}{(2\pi)^2 T} \int_0^T dt \int_{-\infty}^{+\infty} d\omega' \, e^{-i\omega' t} \tilde{p}(\omega') \int_{-\infty}^{+\infty} d\omega'' \, e^{-i\omega'' t} \tilde{p}(\omega'') \int_{-\infty}^{+\infty} d\tau \, e^{i(\omega-\omega'')\tau}, \quad (11)$$

that is:

$$I(\omega) = \frac{1}{2\pi T} \int_0^T dt \int_{-\infty}^{+\infty} d\omega' \, e^{-i\omega' t} \tilde{p}(\omega') e^{-i\omega t} \tilde{p}(\omega). \quad (12)$$

Performing the integral in dt, taking the limit of $T \to +\infty$, and taking advantage of the parity of the integrand with respect to t and of the δ function, $\delta(-\omega - \omega') = \delta(-(\omega + \omega')) = \delta(\omega + \omega')$, we get:

$$I(\omega) = \frac{1}{2T} \tilde{p}(\omega) \tilde{p}(-\omega). \quad (13)$$

Because $p(t)$ is real, the following property holds: $\tilde{p}(-\omega) = \tilde{p}^*(\omega)$. So, the working equation for computing quasiclassical vibrational spectra is:

$$I(\omega) = \frac{1}{2T} |\tilde{p}(\omega)|^2 = \frac{1}{2T} \left| \int_0^T dt \, e^{i\omega t} p(t) \right|^2 . \quad (14)$$

III. RESULTS AND DISCUSSION

We start this Section performing SC calculations on several clusters by means of the ab initio surface. The aim of these calculations is twofold. On the one hand, we demonstrate the accuracy of our approach. On the other hand, we provide a spectroscopic benchmark for water solvation which allows us to estimate the accuracy of our Caldeira-Leggett model. The latter consists of a water molecule coupled to a Caldeira-Leggett bath and we analyze the effect of tuning the strength of the coupling between water and the bath modes. Finally, a close spectroscopic comparison between the approaches based on the Caldeira-Leggett model and the ab initio surface is presented.

A. Water clusters

The first simulations we undertake involve a few water clusters. For the calculations, we employ the accurate MB-pol PES developed by Paesani and coworkers, which has been shown to be able to accurately reproduce the main properties of liquid water.[11, 14, 75] We adopt a total simulation time of 30000 a.u. with a timestep of 5 a.u. To reduce the rovibrational coupling between high-frequency modes and hindered rotations (librations), we follow two different routes. In the first method (MC-DC SCIVR I), we set the initial velocities of all the low-frequency modes (those with harmonic frequencies lower than the bendings) equal to 0. Moreover, at each step of the trajectory we remove the angular momentum and the velocities of each water monomer and rescale the kinetic energies to preserve the desired NVE features. In the second approach (MC-DC SCIVR II), we simply do not evolve the low-frequency modes by setting their positions equal to the corresponding equilibrium values. We benchmark our semiclassical calculations against experiments[76] and MultiMode (MM) or Local Monomer Model (LMM) calculations performed by Bowman and coworkers, when available.[77] Even though these calculations have not been performed on the MB-pol PES but using the WHBB potential,[9, 13] their estimates provide a qualitative benchmark for our simulations due to the top-tier accuracy of both surfaces.

Fig. 1 reports the spectra of the water dimer. It allows to appreciate the main differences between the two methods: MC-DC SCIVR I results in narrower spectral profiles than MC-DC SCIVR II ones, because the angular momentum has been removed from the trajectory. However, MC-DC SCIVR II results in spectra with less numerous side combination peaks, because the combination signals coming from the combined excitation with librational modes are greatly suppressed.

Table I demonstrates that both semiclassical approaches are very accurate in estimating the frequencies of bending and stretching modes, with a mean absolute error (MAE) of 19 and 13 cm^{-1}, when compared to the experiments, and 36 $cm^{-1}$when compared to the MM estimates.

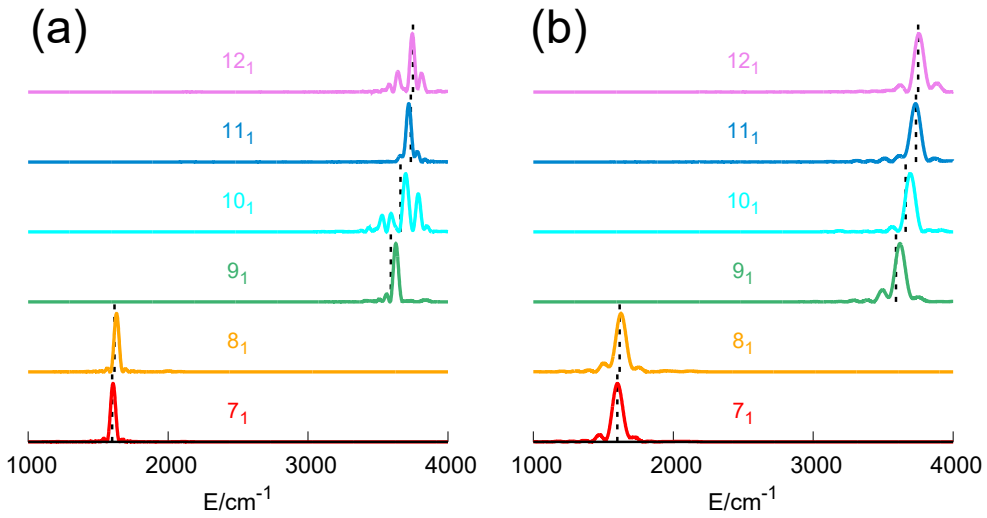

Figure 1. Vibrational power spectra for bending and stretching modes of the water dimer. Panel (a): MC-DC SCIVR I;[60] Panel (b): MC-DC SCIVR II. Black dashed vertical lines: experimental frequencies.

Table I. Fundamental vibrational frequencies for the bendings and stretches of the water dimer (cm^{-1}). Under column "Mode" we report the index of the vibrational normal modes sorted according to their increasing harmonic frequency. The second column reports the experimental frequencies. The third column shows the MultiMode (MM) estimates. Under columns "MC-DC SCIVR I" and "MC-DC SCIVR II" we report the semiclassical estimates obtained in this work. The last column shows the harmonic frequencies. The last two rows report the Mean Absolute Errors (MAEs) with respect to the experimental (MAE exp) and Multimode (MAE MM) values.

Mode	**Exp**	**MM**	**MC-DC SCIVR I**	**MC-DC SCIVR II**	**Harm**
7	1600	1588	1607	1601	1651
8	1617	1603	1632	1626	1665
9	3591	3573	3627	3620	3752
10	3661	3627	3698	3694	3832
11	3734	3709	3720	3731	3915
12	3750	3713	3745	3755	3935
MAE exp	-	23	19	13	133
MAE MM	-	-	36	36	156

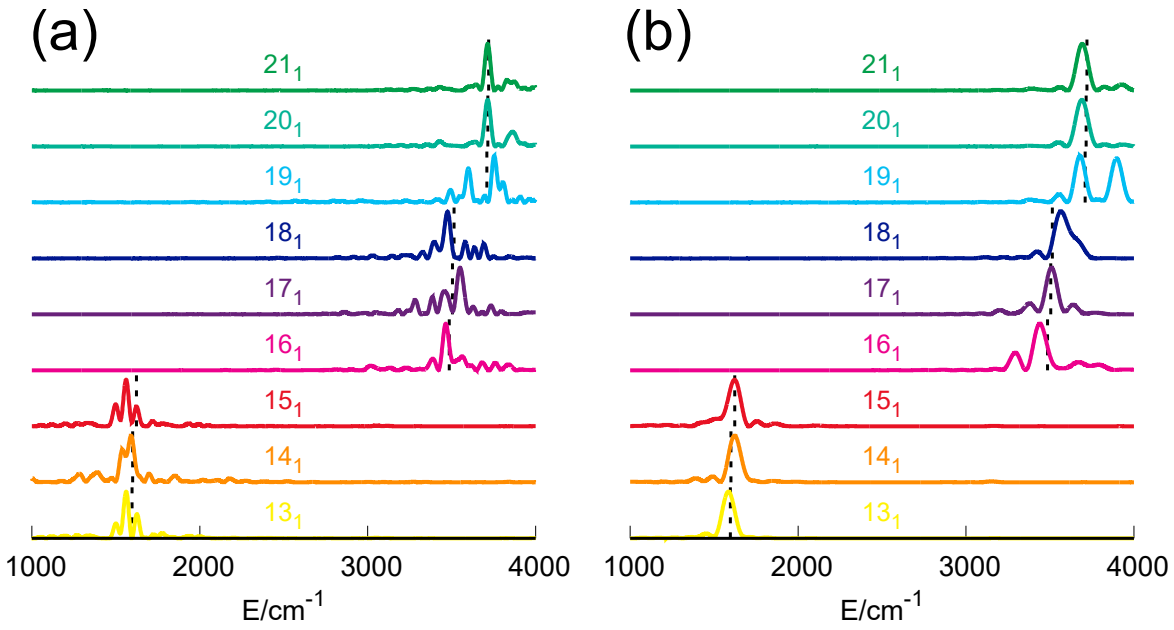

Figure 2. Vibrational power spectra for bending and stretching modes of the water trimer. Panel (a): MC-DC SCIVR I[60]; Panel (b): MC-DC SCIVR II. Black dashed vertical lines: MM estimates.

These conclusions are confirmed by the analysis of the water trimer, whose spectra are reported in Fig. 2. Again, MC-DC SCIVR II results in cleaner signals but with broader peaks. However, a few combination bands and overtones are still present in MC-DC SCIVR II: Those signals are evident for instance for the peaks associated with modes 18 and 19.

Both methods are very accurate as it can be seen from Table II, which presents frequency estimates for bendings and stretches. Experimental values for the trimer have not been reported because, at best of our knowledge, they are incomplete. When compared to the MM calculations, MC-DC SCIVR I shows on average an error of 29 cm^{-1}, while the second approach displays a MAE of 28 cm^{-1}. These values are comparable to those reported for the dimer, for which agreement with the experiments is within 20 cm^{-1}and slightly worse with MM.

Table II. Fundamental vibrational frequencies for bendings and stretches of the water trimer (cm^{-1}). Labels are chosen in agreement with Table I.

Mode	MM	MC-DC SCIVR I	MC-DC SCIVR II	Harm
13	1597	1562	1585	1656
14	1600	1591	1622	1661
15	1623	1561	1622	1685
16	3486	3465	3439	3636
17	3504	3550	3509	3685
18	3514	3475	3565	3694
19	3709	3753	3679	3906
20	3716	3714	3690	3915
21	3720	3714	3692	3916
MAE MM	-	29	28	143

We now move to the water hexamer prism, which is the lowest-dimensional water cluster showing a three-dimensional structure and for this reason it has been dubbed to be the smallest water droplet.[6] Fig. 3 reports the spectra of $(H_2O)_6$ obtained using our two MC-DC-SCIVR approaches.

The results are analogous to the ones obtained for lower-dimensional clusters: MC-DC SCIVR I returns more resolved peaks but the presence of the low-frequency modes causes the appearance of numerous side peaks associated to overtones and combination signals. MC-DC SCIVR II shows instead cleaner signals, where some combination bands are clearly present, as it can be seen for example by looking at the peak associated to mode 43. Similarly to the other clusters, the MC-DC SCIVR II spectra are broader because the angular momentum has not been removed from the trajectory. Table III reports the frequencies and the MAE of the two approaches with respect to the LMM calculations. Even in this case, both methods provide similar results and the deviation from other types of calculations are similar to the ones obtained for the trimer. Specifically, with respect to LMM calculations, MC-DC SCIVR I has a MAE of 25 cm^{-1}, while MC-DC SCIVR II shows a MAE of 31 cm^{-1} .

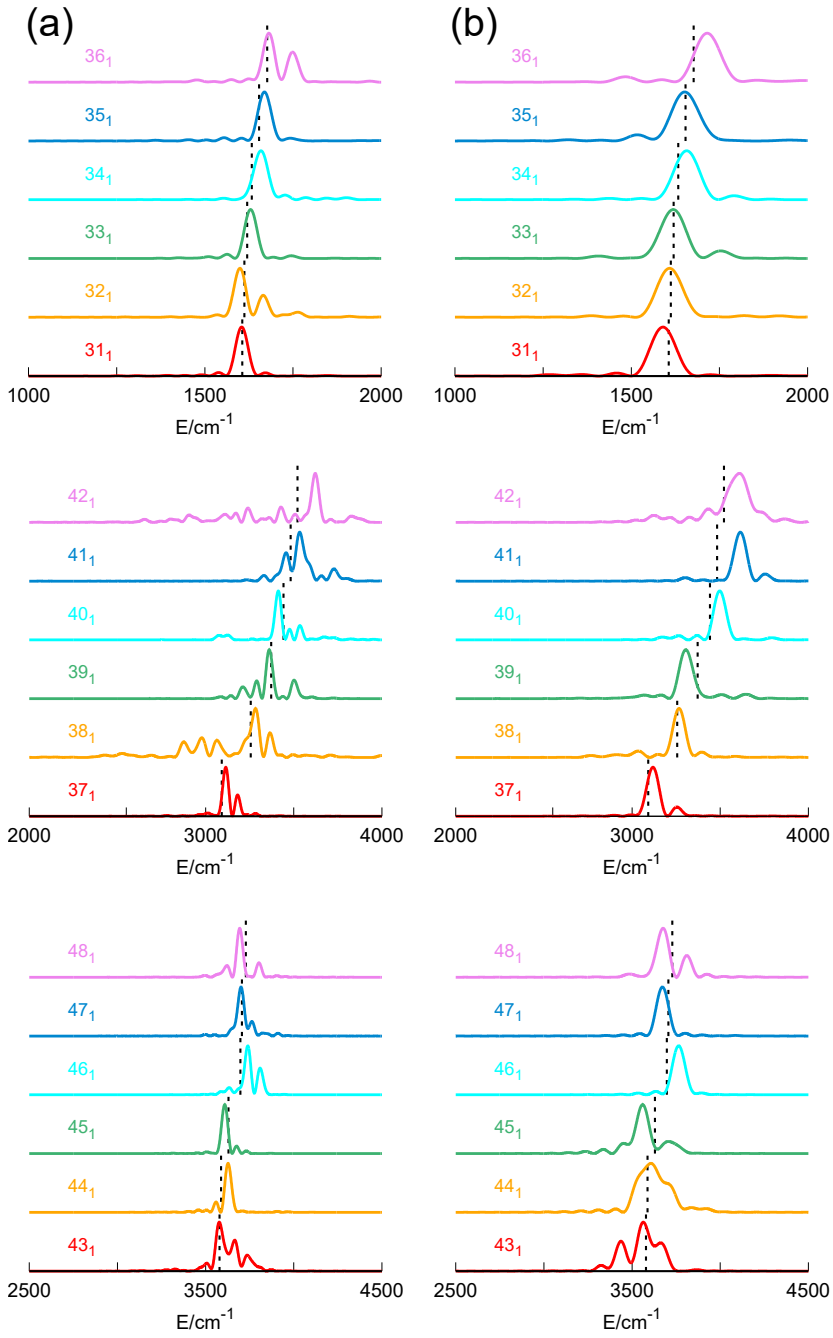

Figure 3. Vibrational power spectra of the water hexamer prism. Panel (a): MC-DC SCIVR I;[60] Panel (b): MC-DC SCIVR II. Black dashed vertical lines: Local Monomer Model (LMM) estimates.

Table III. Fundamental vibrational frequencies for bendings and stretches of the water hexamer prism (cm^{-1}). Under column "LMM" we have reported the Local Monomer Model estimates, obtained using the WHBB PES. The other labels are chosen in agreement with Table I.

Mode	**LMM**	**MC-DC SCIVR I**	**MC-DC SCIVR II**	**Harm**
31	1606	1605	1590	1652
32	1612	1600	1609	1671
33	1620	1630	1619	1680
34	1633	1659	1649	1690
35	1654	1669	1652	1711
36	1677	1682	1715	1729
37	3092	3114	3118	3307
38	3256	3283	3266	3513
39	3372	3361	3305	3603
40	3442	3412	3463	3627
41	3482	3534	3423	3729
42	3521	3622	3556	3747
43	3579	3578	3564	3789
44	3588	3627	3607	3805
45	3630	3609	3560	3818
46	3697	3739	3764	3908
47	3706	3701	3672	3910
48	3728	3694	3676	3911
MAE LMM	-	25	31	161

The last water cluster we have studied is $(H_2O)_{21}$. This system is of remarkable interest because very recent and detailed spectroscopic studies point at this cluster as the smallest one for which a single water molecule (the one located at the center of the cluster) can be considered as fully solvated, i.e. the spectral features of the central molecule match those of bulk liquid water.[60] Therefore, the bending and stretching frequency values of the central molecule will provide our "condensed-phase" ab initio fingerprints. In Fig. 4 (a) we report the cluster structure and highlight

the central monomer. From the spectroscopic point of view, to label a water molecule as solvated, one must take into account all the spectroscopic signals generated by that specific monomer. The medium and high-energy part of the liquid water IR spectrum is mainly characterized by the signal of the bending, located at 1640 cm^{-1}, the broad band of the stretches, which spans the region from 3000 to 3500 cm^{-1}, and the combination band of bending and librations that generates a band at around 2100 cm^{-1}. We choose not to consider the low-frequency portion of the IR spectrum (below 1000 cm^{-1}) because in this spectral region the experiment almost displays a continuum of signals. To be able to describe also the combination band, the method labeled as MC-DC SCIVR I is the method that has to be applied to tackle this problem. In fact, differently from MC-DC SCIVR II, in the MC-DC SCIVR I approach all low-frequency modes are evolved in time.

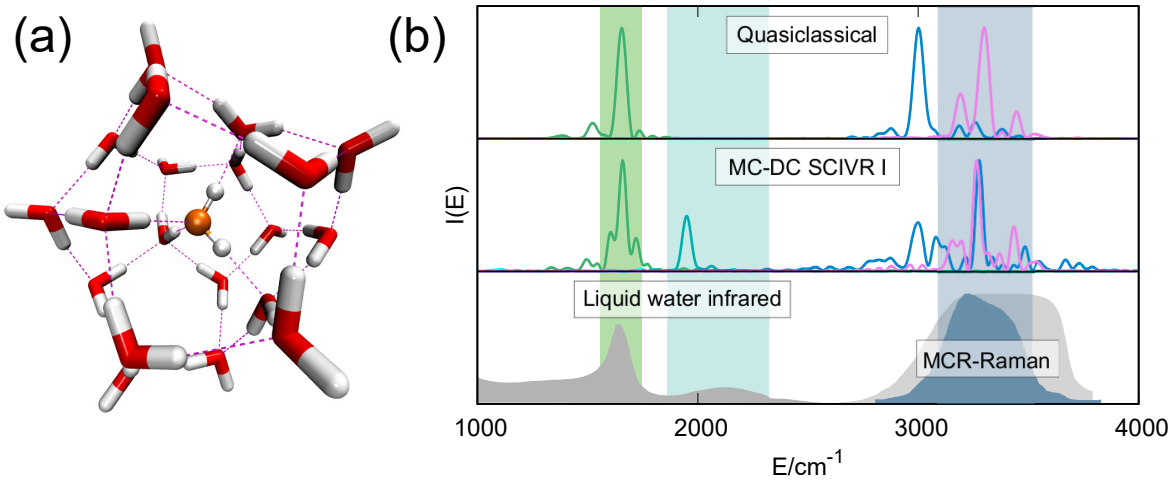

Figure 4. Panel (a): Structure of $(H_2O)_{21}$, where the central monomer is highlighted in orange. Panel (b): Vibrational spectra originated from the central monomer of $(H_2O)_{21}$ and comparison with liquid water experiments. Top: quasiclassical spectrum; middle: MC-DC-SCIVR I spectrum taken from Ref. [60]; bottom: liquid water IR spectrum (gray) and MCR-Raman experiment (blue).[78] The intensity of the combination band has been scaled to better appreciate it.

In Fig. 4 we report the spectrum of the stretches, bending, and combination band of the central water monomer of the $(H_2O)_{21}$ cluster. All the vibrational signals associated to this target monomer match the corresponding liquid water infrared bands. Moreover, the stretches are in agreement with Multiple Curve Resolution-Raman experiments, which identify the portion of the stretching band generated by tetrahedrally coordinated water molecules.[78] These observations lead to the conclusion that the central monomer of $(H_2O)_{21}$ is completely solvated.[60] We also observe that

the energy splitting between the stretches tend to vanish.

To highlight the importance of the inclusion of the quantum nuclear effects in water molecular dynamics simulations, in Fig. 4 we have reported the quasiclassical power spectrum for the same system. The first feature we observe is that combination bands cannot be obtained through classical simulations. In fact, the quasiclassical power spectrum is the result of a classical approach, i.e. the Fourier transform of a velocity-velocity correlation function (see Eq. 14) is performed. The absence of the combination band in the quasiclassical spectrum points to the necessity of having a quantum approach to study the water solvation process. Then, it is interesting to notice that one of the peaks associated to the stretching motions in Fig. 4 is strongly red shifted in the quasiclassical simulation with respect to the semiclassical one. Since our quasiclassical and semiclassical vibrational spectra are based on the same trajectory, i.e. phase-space points, we conclude that the different spectroscopic picture is due to nuclear quantum effects.

B. Spectroscopic analysis of the Caldeira-Leggett model

We now consider the basic Caldeira-Leggett model.[16] The corresponding Hamiltonian is

$$\mathcal{H} = \mathcal{H}_s + \sum_{i=1}^{F_b} \left\{ \frac{p_i^2}{2} + \frac{1}{2}\Big[\omega_i y_i + \frac{c_i}{\omega_i}\left(s - s_{eq}\right)\Big]^2 \right\}, \tag{15}$$

where F_b is the number of bath DOFs, whose positions are y_i, p_i are the momenta, and ω_i are the harmonic frequencies of the bath. s is the position of the system and s_{eq} the corresponding equilibrium value, while c_i are the coupling coefficients. All positions and momenta have been mass-scaled. In the previous equation, $\mathcal{H}_s$ is the monodimensional Hamiltonian of the system

$$\mathcal{H}_s = \frac{p_s^2}{2} + D_e\left(1 - e^{-\alpha(s-s_{eq})}\right)^2, \tag{16}$$

being p_s the momentum of the system. The dissociation energy D_e, α, and s_{eq} are chosen in agreement with ref. [79], so that the system represents the I_2 molecule, which is modeled by means of a Morse potential. In our simulations we consider an Ohmic bath with exponential cutoff.[80] The corresponding spectral density is

$$J_e(\omega) = \eta\omega e^{-\frac{\omega}{\omega_c}}, \tag{17}$$

in which ω_c is the cutoff frequency of the bath and η is a quantity describing the strength of the coupling. The bath frequencies can be discretized through adoption of a discrete spectral density

$$J(\omega) = \frac{\pi}{2} \sum_{i=1}^{F_b} \frac{c_i^2}{\omega_i} \delta(\omega - \omega_i), \tag{18}$$

where the coupling coefficients c_i are chosen as follows[81]

$$c_i^2 = \frac{2}{\pi} \omega_i \frac{J_e(\omega_i)}{\rho(\omega_i)}. \tag{19}$$

In this way, this discrete representation will match the continuous one if F_b reaches infinity. $\rho(\omega)$ is the frequency density

$$\int_0^{\omega_i} d\omega \, \rho(\omega) = i, \qquad i = 1, \ldots, F_b, \tag{20}$$

chosen as

$$\rho(\omega) = a \frac{J_e(\omega)}{\omega}. \tag{21}$$

In the previous equation, a is a normalization coefficient ensuring that $i = F_b$ if the largest frequency $\omega_i = \omega_{max}$ is selected in Eq. (20) and it is equal to

$$a = \frac{F_b}{\eta \omega_c \left(1 - e^{-\frac{\omega_{max}}{\omega_c}}\right)}. \tag{22}$$

Inserting Eq. (17) and Eq. (22) into Eq. (21) and applying Eq. (20), it is possible to derive the working equation for selecting the bath discrete frequencies

$$\omega_i = -\omega_c \ln \left[1 - \frac{i}{F_b} \left(1 - e^{-\frac{\omega_{max}}{\omega_c}}\right)\right], \qquad i = 1, \ldots, F_b. \tag{23}$$

In our simulations we employ 2^{14} steps of $0.1\pi/\omega_s$ a.u..

We start by benchmarking our MC-DC-SCIVR calculations against exact quantum mechanical results, obtained with the splitting operator approach,[79] and against full-dimensional semiclassical simulations obtained by applying the TA-SCIVR and MC-SCIVR methods. For the TA-SCIVR spectra we use 10^4 trajectories to fully converge the results. For the Caldeira-Leggett simulations we set the spectral resolution equal to $1/T$. We test our semiclassical approach against various

Caldeira-Leggett models by varying the strength of the coupling, the cutoff frequency, and choosing resonant or non-resonant bath modes. In Fig. 5 we report the spectra obtained for 2- and 3-dimensional Caldeira-Leggett models. We define the quantity η_{eff} as the ratio between η and the harmonic frequency of the system ω_s.

First of all, it is possible to appreciate the accuracy of the semiclassical methods for these systems, because the agreement with the exact simulations is always very good for all the models examined. Here, we employ the MC-DC-SCIVR simulation to look at the one-dimensional subspace of the system and to calculate its spectrum. This partial spectrum turns out to be as accurate as the full-dimensional semiclassical ones. This is not surprising considering that in the divide-and-conquer approach the trajectories are full dimensional. This exercise can be indifferently replicated for any vibrational subspace, including those for the degrees of freedom of the bath. By recalling that the MC-DC-SCIVR spectra were obtained using only one classical trajectory and the Hessians have been calculated in this case only for the one-dimensional system, we can appreciate the huge computational speedup provided by MC-DC SCIVR. The results also show that the projection procedure greatly reduces the number of signals coming from the bath excitations, simplifying the interpretation of the spectrum.

Having established the accuracy of MC-DC SCIVR versus exact quantum dynamics calculations for low-dimensional baths, we can now move to systems with more bath DOFs. For higher-dimensional baths, exact quantum mechanical results are not available, hence the MC-DC-SCIVR spectra have been compared only with full-dimensional semiclassical simulations. In Fig. 6 we report the spectra for F_b ranging from 5 to 100. For 5- and 10-dimensional baths the full-dimensional semiclassical spectra present a huge number of peaks originated from the fundamental and overtone transitions, with the addition of the presence of the combination bands associated to the bath. Nevertheless, the MC-DC-SCIVR spectra are still accurate, and the projection procedure allows to greatly reduce the intensities of the peaks associated to the bath DOFs. When the dimensionality of the bath reaches 20, the curse of dimensionality kicks in and both TA SCIVR[24] and the single-trajectory MC SCIVR fail to provide a numerically converged spectrum, while the MC-DC-SCIVR spectrum is clear and perfectly detectable. This happens because the full-dimensional system is characterized by so many DOFs that the time-dependent overlap in Eq. (1) cannot be longer obtained from full-dimensional simulations in a reasonable amount of computational time. Instead, by using our MC-DC-SCIVR approach we are able to recover clear signals for the I_2 system, even in the case of 100 bath DOFs.

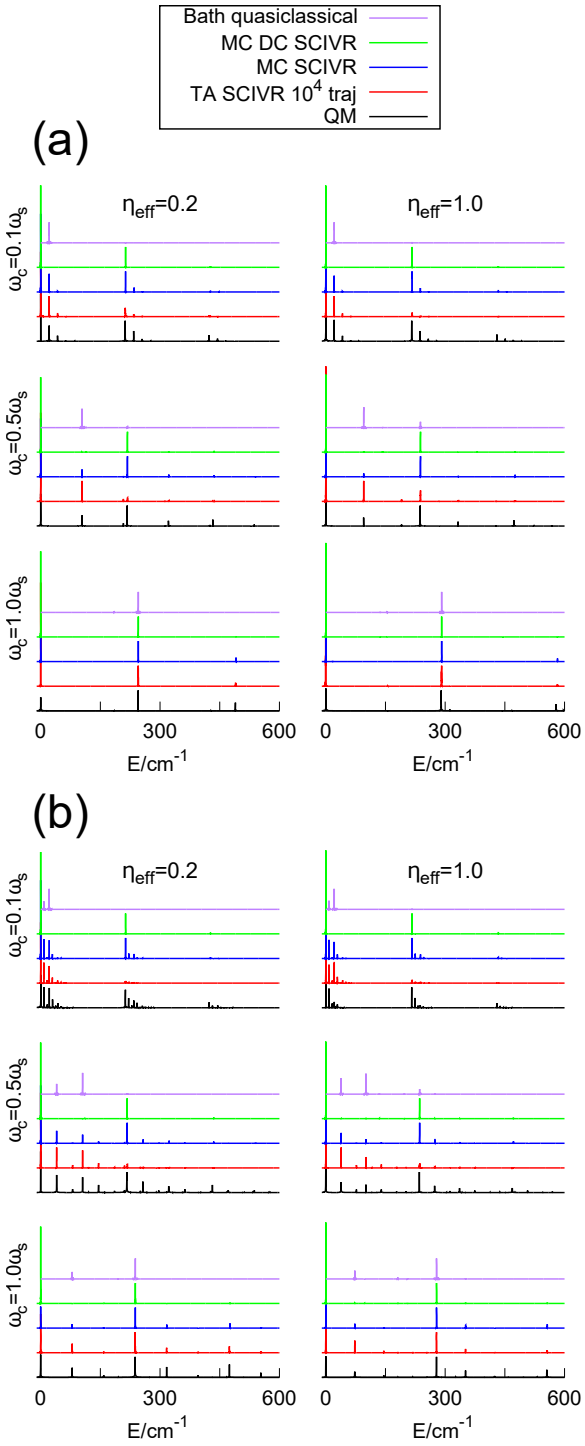

Figure 5. Vibrational power spectra of the Caldeira-Leggett model. (a) Spectra in the case of one-dimensional baths. (b) Spectra for two-dimensional baths. Black lines: exact quantum mechanical spectra.[79] Red lines: TA-SCIVR estimates. Blue lines: MC-SCIVR spectra. Green line: MC-DC-SCIVR spectra. We have also added the bath quasiclassical spectra (purple line) to help the reader to identify the peaks of the bath DOFs. In quantum and semiclassical spectra zero point energies have been shifted to 0. In all the examples $\omega_{max} = \omega_c$.

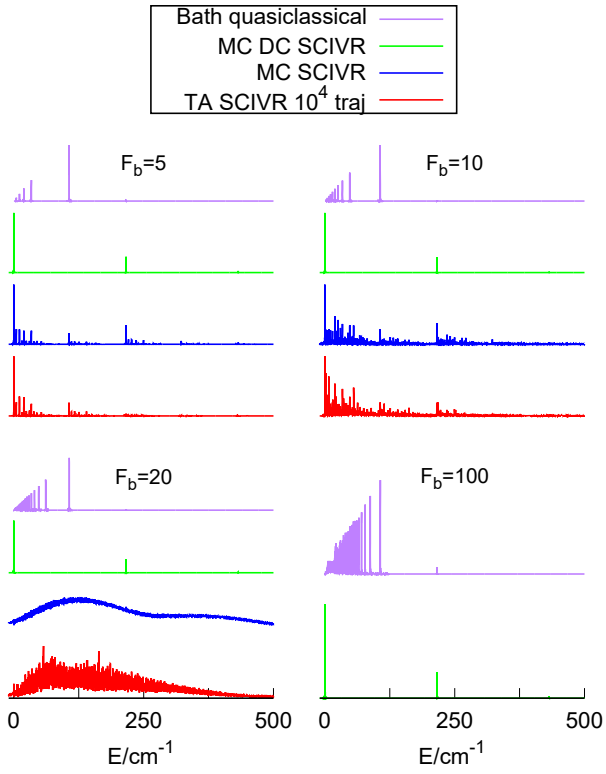

Figure 6. Vibrational power spectra of the Caldeira-Leggett model. The parameters have been chosen as follows: $\eta_{eff} = 0.5$, $\omega_c = 0.1\omega_s$, and $\omega_{max} = 0.5\omega_s$. Top left: 5-dimensional bath ($F_b = 5$). Top right: 10-dimensional bath ($F_b = 10$). Bottom left: 20-dimensional bath ($F_b = 25$). Bottom right: 100-dimensional bath ($F_b = 100$). Colors and labels have been chosen in agreement with Fig. 5.

C. Water coupled to the Caldeira-Leggett bath

After demonstrating the excellent accuracy of semiclassical methods for the Caldeira-Leggett model, we build a model potential for solvation made of a water molecule coupled to the bath. This model will allow us to understand the level of accuracy of a Caldeira-Leggett bath in describing a condensed-phase environment, where a central water molecule is solvated. Previous calculations for the $(H_2O)_{21}$ cluster serve for a quantitative comparison. In this case, for the water part of the potential we adopt the accurate PES developed by Thiel and coworkers,[82] a full-dimensional surface in Cartesian coordinates that provides well resolved semiclassical signals for the fundamentals at 1608, 3732, and 3814 cm^{-1} for the bending, symmetric and asymmetric stretches, respectively. Furthermore, each of the three vibrational normal modes of water is bilinearly coupled

to the harmonic bath in a way that is similar to the one adopted for the I_2 molecule in Sec. III B, so that a third of the bath modes were coupled to the bending, a third to the symmetric stretch and a third to the asymmetric one. More specifically, the bath modes whose frequencies are extracted from Eq. (23), are coupled alternatively to the bending, symmetric stretch, and asymmetric stretch of the water molecule. This setup somehow mimics the interactions of a water molecule in the water solvent and it will be compared in Section III D to the spectroscopic features of a single water molecule embedded in a water cluster. In this Section, we introduce $\omega_{max,eff}$, η_{eff}, and $\omega_{c,eff}$ as the ratio between the actual values of the corresponding parameters and the highest harmonic frequency of the bare water molecule (the one of the asymmetric stretch). For all simulations, the dynamics is carried out using a total simulation time of 30000 a.u. and a time step of 10 a.u..

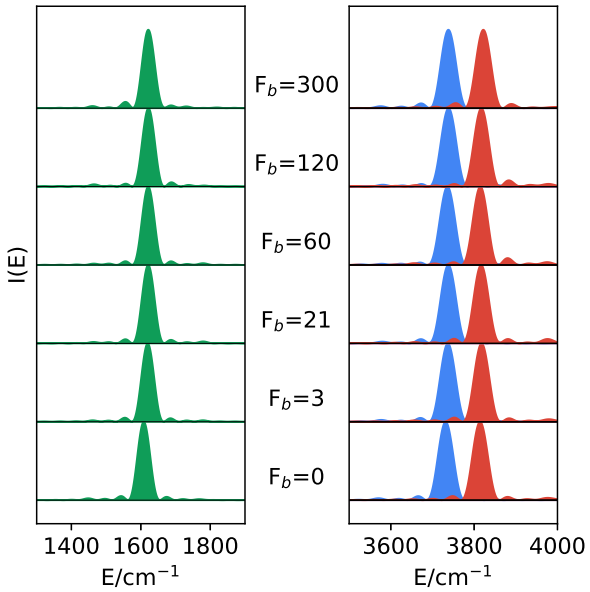

Figure 7. MC-DC-SCIVR power spectra of a water molecule coupled to the Caldeira-Leggett bath, performed at different dimensionalities of the bath. The green signals identify the bendings of the water molecule. In blue and red we highlight the symmetric and asymmetric stretches, respectively. The other parameters are selected as follows: $\eta_{eff} = 0.1$, $\omega_{c,eff} = 0.1$, and $\omega_{max,eff} = 0.5$.

In Fig. 7 we report the results. In the calculations, η_{eff} and $\omega_{c,eff}$ are set equal to 0.1, while $\omega_{max,eff} = 0.5$. The number of bath DOFs varies from 0 up to 300. Overall, we observe that the harmonic bath does not change the frequencies of the water molecule significantly. The bending slightly blueshifts when coupled to the harmonic bath and the stretches remain quite constant.

When compared to the experimental band of liquid water, the stretches are way too blueshifted and not compatible with the ones of a solvated water molecule.

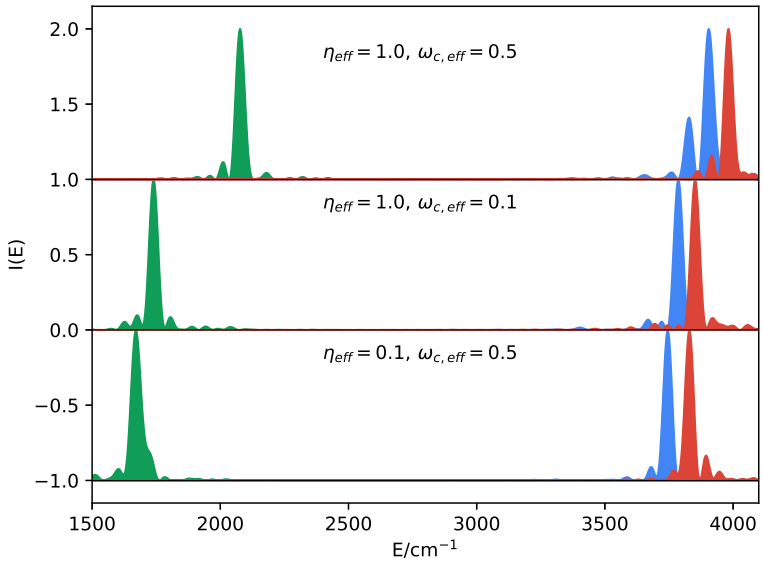

Figure 8. MC-DC-SCIVR power spectra of a water molecule coupled to the Caldeira-Leggett bath in the case of $F_b = 300$, performed for different combinations of the other parameters of the model. The green signals identify the bendings of the water molecule. In blue and red we highlight the symmetric and asymmetric stretches, respectively. $\omega_{max,eff}$ is set equal to 0.5.

Before rushing into conclusions that the Caldeira-Leggett model is not suitable to describe the spectroscopy properties of water solvation, a couple of additional aspects needs to be investigated. First one could try to regain the expected red shift of frequencies by increasing the coupling between the water molecule and the bath. Then, one should also study the effect of the spectral density on the results by substituting the Ohmic model with the actual spectral density of liquid water. To further investigate the influence of the parameters on the vibrational frequencies of the system, we compute the vibrational power spectra of this model for different combinations of the Caldeira-Leggett parameters. In Fig. 8 we report the results in the case of $F_b = 300$ and Ohmic bath. In none of these cases we find signals typical of a solvated water molecule. When η_{eff} and $\omega_{c,max}$ increase, the vibrational frequencies of the water molecule progressively blueshift up to values that are inconsistent with the ones of bulk liquid water and sometimes even higher than the harmonic estimates for the isolated molecule. This trend is opposite to the expected one, showing

that a tuning of the Caldeira-Leggett model parameters in addition to being an unwanted *ad-hoc* procedure is unlikely to provide correct results. For this reason, in the following we will set η_{eff} and $\omega_{c,eff}$ equal to 0.1.

Upon having established that the model potential "as is" cannot reproduce the vibrational features of bulk water, we consider a more realistic environment from which to select the bath frequencies. Unfortunately, the experimental liquid water IR spectrum does not seem a good distribution to sample the density of vibrational states from. In fact, the intensities are driven by the dipole moment derivatives, i.e. dark transitions are not accounted for, and cannot be easily related to the number of oscillators. Therefore, instead of relying on the analytical formula of Eq. (23), to extract the bath frequencies we employ the classical vibrational density of liquid water computed by Marsalek and Markland using on-the-fly ab initio molecular dynamics at the level of hybrid density functional theory (DFT).[83] In practice, the digitized distribution is fitted with cubic splines. Then, we apply the standard von Neumann technique to sample the bath harmonic frequencies. In this way, we not only have a more realistic and accurate frequency distribution, but we also remove a parameter from the simulation, i.e. $\omega_{max,eff}$ the maximum frequency of the bath. The distribution and the histogram of the sampled frequencies are reported in the inner panel of Fig. (9). In the outer panel of the same figure, we have reported the semiclassical vibrational spectra for different bath dimensionalities. We observe a more structured spectrum for the stretches, probably because of the higher number of bath frequencies in the same energy window. The bending blueshifts as the number of bath DOFs increases, which is consistent to what is observed for water when moving from the gas phase to the liquid one and already captured in Fig. 7. However, the stretching frequencies (and the bending frequencies for high values of F_b) are too blueshifted and thus do not quantitatively represent the vibrational features of a solvated water molecule, in contrast with the ab initio potential approach presented in Sec. III A.

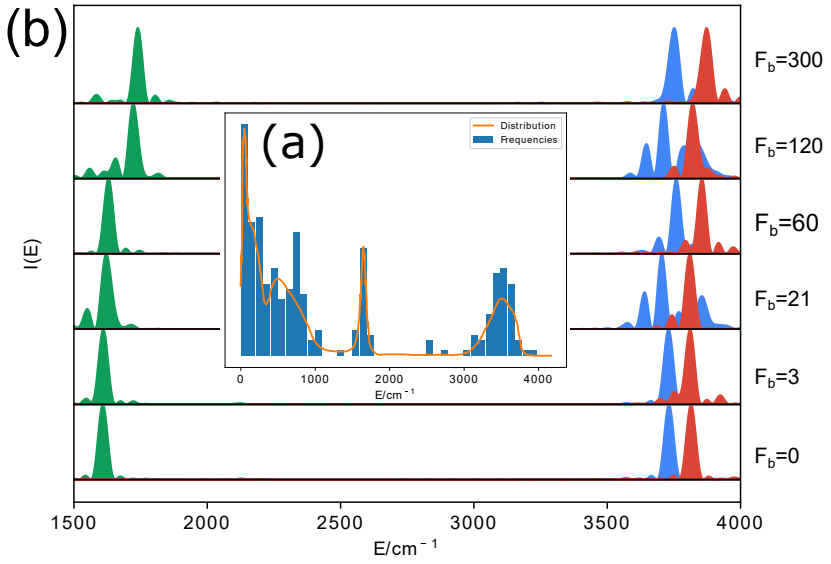

Figure 9. Semiclassical vibrational power spectra of the water molecule coupled to the harmonic bath whose frequencies are extracted from the liquid water vibrational density of states of Ref. 83. Panel (a): vibrational frequency distribution (orange) and histogram of the sampled frequencies (blue). Panel (b): MC-DC-SCIVR vibrational spectra performed for different dimensionalities (F_b) of the bath. Bending (green), symmetric (blue) and asymmetric (red) stretch signals are reported.

To provide a tighter comparison between the model and the ab initio potential, we also consider a different probability distribution. We compute the complete quasiclassical vibrational spectrum of $(H_2O)_{21}$ (total propagation time $T = 30000$ a.u. with a time step of 5 a.u.) and apply the procedure described earlier to sample the bath harmonic frequencies. The quasi-classical spectrum and the histogram of the extracted frequencies are reported in the inner panel of Fig 10. While the spectral regions spanned by this new distribution are similar to those of the liquid, the relative intensities are remarkably different from the ones of Fig. 7. In the outer panel of Fig. 10 we report the semiclassical spectra computed at different values of F_b. Similarly to the other cases, the frequency of the bending generally blueshifts as the number of bath DOFs increases. For the stretches, a similar behavior is recovered, in contrast to what happens in water cluster simulations.

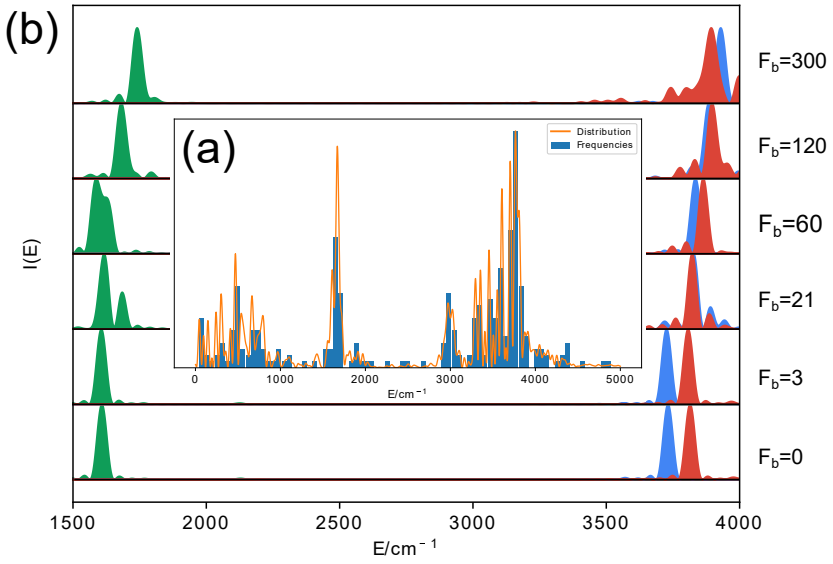

Figure 10. Vibrational power spectra of the water molecule coupled to the harmonic bath whose frequencies are extracted from the $(H_2O)_{21}$ vibrational density of states. Panel (a):vibrational frequency distribution (orange) and histogram of the sampled frequencies (blue). Panel (b): MC-DC-SCIVR vibrational spectra performed for different dimensionalities of the bath. Bending (green), symmetric (blue) and asymmetric (red) stretch signals are reported.

D. Caldeira-Leggett model versus ab initio potential

We are now ready to compare the two approaches presented above in terms of spectroscopic accuracy with respect to the experimental IR spectrum of liquid water. Panels (a) and (b) of Fig. 11 show how the frequencies of the fundamental stretching and bending normal modes change when different spectral densities and bath dimensionalities are employed. In panel (b) we observe two distinct trends. In the case of the Ohmic sampling, the bending frequency varies mostly right after the addition of the bath modes and then it remains constant as the dimensionality of the bath is increased. In contrast, when more realistic distributions are used to sample the bath frequencies, we generally observe a blueshift of the bending frequency as the number of bath DOFs increases. The major deviation from the gas phase value is about +130 cm^{-1}. For the bending, the bulk water experimental frequency does not differ significantly from the gas-phase value (1640 vs 1590 cm^{-1}). Therefore, the bending estimates of the model potential lie within the experimental energy

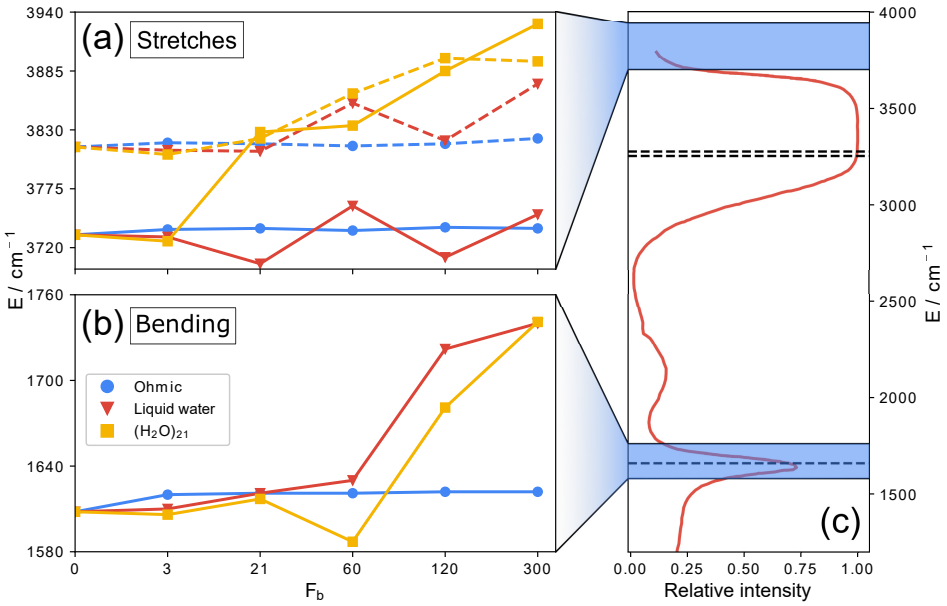

Figure 11. Comparison between the model composed of a water molecule coupled to the Caldeira-Leggett potential and the high-energy portion of the experimental IR spectrum of liquid water. Bath frequencies are sampled using Eq. (23) (blue), the liquid water vibrational density of states calculated by Marsalek and Markland (red), and the $(H_2O)_{21}$ vibrational density of states (yellow). Panel (a): asymmetric (dashed lines) and symmetric (continuous lines) stretching frequencies at growing bath dimension. Panel (b): same but for the bending frequency. In panel (c) the experimental liquid water spectrum is shown in red. The light blue areas represent the regions spanned by the calculated frequencies of the Caldeira-Leggett model. The MC-DC-SCIVR I frequency estimates for bending and stretches of the central water molecule of $(H_2O)_{21}$ are reported as black dashed horizontal lines.

window reported in panel (c). In panel (a), the frequency variations of the symmetric (continuous lines) and asymmetric (dashed lines) stretching modes for different approaches to sample the frequencies and for different bath dimensionalities are reported. When Eq. (23) is applied to sample the bath frequencies, the results are similar to the ones of the bending with a small dependence on the parameter F_b. Conversely, when a different frequency probability distribution is considered, we observe different trends. For both stretches in the case of Markland's DFT liquid water frequency distribution we observe fluctuations of the frequencies, with the tendency to increase the vibrational energy of the asymmetric stretch when more harmonic oscillators are coupled to

the water molecules. In the case of the $(H_2O)_{21}$ distribution, instead, we have that the calculated frequencies of both the stretches keep on increasing when more harmonic oscillators are added to the bath. This blueshift causes the frequency difference between symmetric and asymmetric stretch to almost disappear in the case of 21 and 120 bath DOFs. The deviations of the stretching frequencies with respect to the center of the liquid water stretching range between 400 and 600 cm^{-1} . So, the Caldeira-Leggett values fall outside the experimental window in spite of its substantial width. On the contrary, as already observed above for the $(H_2O)_{21}$ cluster, panel (c) of Fig. 11 shows how both stretching and bending frequencies are within the experimental windows when calculated with the ab initio potential. This confirms the importance of employing an accurate potential, in which all many-body potential interactions are taken into account.

From the qualitative point of view, increasing the number of bath modes results in an increase of the frequency of the bending when a realistic probability distribution is used to sample the bath frequencies. This effect is also observed in IR experiments. In fact, the bending frequency blue-shifts from 1590 cm^{-1} in the gas phase to 1640 cm^{-1} in the liquid. The fact that the model is able to capture both the qualitative and quantitative behaviors of the bending mode is a source of potential interest. In fact, in the recent literature it has been pointed out that the in-depth analysis of the bending mode could be a powerful tool to study the hydrogen bond structure in aqueous systems.[4] Concerning the stretches, their experimental IR signals strongly redshift when going from the gas to the liquid phase. Unfortunately, this peculiar characteristic is not found in the Caldeira-Leggett model potential, which predicts that stretches are blueshifted with respect to their gas-phase counterparts.

IV. SUMMARY AND CONCLUSIONS

In this paper, we have demonstrated once more that MC-DC SCIVR is a powerful quantum mechanical tool to study the (micro-)solvation process from the spectroscopic point of view. Our semiclassical study of water clusters of increasing dimensionality, by means of a highly accurate ab initio potential, permitted a comparative study with experiments to identify the fingerprints of solvation. We applied two modified versions of MC-DC SCIVR to the study of water clusters. For low-dimensional clusters, we confirmed the accuracy of the methods by comparing our simulation with experiments, MultiMode, and Local Monomer calculations.

The spectrum of $(H_2O)_{21}$ served as a benchmark for studying the effectiveness of a solvation

model made of a central water molecule described by means of an accurate PES and a harmonic bath coupled to the central molecule through the Caldeira-Leggett prescription. Eventually, we found that the results based on the ab initio surface are consistent with the experimental picture both qualitatively and quantitatively. The Caldeira-Leggett model is instead reliable in mimicking the condensed phase environment only for the bending motion, which it does not actually shift significantly (only 50 cm^{-1}) from the gas-phase value. Since the Caldeira-Leggett simulation is by far computationally cheaper than the ab initio-based one, this suggests that looking at the bending signals of a potentially solvated molecule could be a convenient way to detect and better understand solvation.

Furthermore, on the basis of the computationally cheap model, we analyzed the frequency shifts of the water signals due to the interaction with the bath. We found that the blueshift of the bending associated with the gas-liquid transition is correctly reproduced if a realistic probability distribution is employed to sample the harmonic frequencies. Conversely, the red shift of stretching modes is not found anyway, and the frequency values are hundreds of wavenumber higher than the center of the corresponding experimental band. Interestingly, we have found that the frequencies of the stretches can degenerate if the $(H_2O)_{21}$ frequency distribution is employed to sample the Caldeira-Leggett bath harmonic frequencies. This feature has been observed also in the ab initio simulations of $(H_2O)_{21}$ and in those of a water molecule adsorbed on titania surfaces.[59] The latter supramolecular system is characterized by the co-presence of the water modes and a huge number of titania phonons, thus resembling the model we are studying here.

We have performed quasiclassical spectroscopic investigations as well. A comparison between these and the semiclassical spectra reveals the importance of nuclear quantum effects for a better description of the water solvation process. Specifically, we have shown that the combination band between the bending mode of the central water molecule and the network librations, which is key in defining the solvation regime of water, can be described only if a quantum (semiclassical) approach is undertaken.

In conclusion, this study establishes MC-DC SCIVR as an accurate and reliable technique to study (micro-)solvation at the molecular scale. It can deal with high dimensional systems and it takes into account quantum mechanical effects typical of hydrogen-bonded systems like water and water clusters. This shows that the method can be employed to assess the accuracy of potential models, force fields, PESs, or on-the-fly dynamics. In the future, we plan to apply MC-DC SCIVR to study solvation and microsolvation of several species, including biological ones. In fact, MC-

DC-SCIVR calculations can be performed on-the-fly if a full-dimensional PES is not available.

DATA AVAILABILITY

The data that support the findings of this study are available from the corresponding author upon reasonable request.

ACKNOWLEDGMENTS

Authors acknowledge financial support from the European Research Council (Grant Agreement No. (647107)—SEMICOMPLEX—ERC- 2014-CoG) under the European Union's Horizon 2020 research and innovation programme, and from the Italian Ministry of Education, University, and Research (MIUR) (FARE programme R16KN7XBRB- project QURE).

[1] T. Yagasaki and S. Saito, Annu. Rev. Phys. Chem. **64**, 55 (2013).

[2] M. Śmiechowski, C. Schran, H. Forbert, and D. Marx, Phys. Rev. Lett. **116**, 027801 (2016).

[3] N. Yang, C. H. Duong, P. J. Kelleher, A. B. McCoy, and M. A. Johnson, Science **364**, 275 (2019).

[4] T. Seki, K.-Y. Chiang, C.-C. Yu, X. Yu, M. Okuno, J. Hunger, Y. Nagata, and M. Bonn, J. Phys. Chem. Lett. (2020).

[5] M. Ceriotti, W. Fang, P. G. Kusalik, R. H. McKenzie, A. Michaelides, M. A. Morales, and T. E. Markland, Chem. Rev. **116**, 7529 (2016).

[6] J. O. Richardson, C. Pérez, S. Lobsiger, A. A. Reid, B. Temelso, G. C. Shields, Z. Kisiel, D. J. Wales, B. H. Pate, and S. C. Althorpe, Science **351**, 1310 (2016).

[7] J. Liu, W. H. Miller, G. S. Fanourgakis, S. S. Xantheas, S. Imoto, and S. Saito, J. chem. Phys. **135**, 244503 (2011).

[8] X. Liu and J. Liu, Mol. Phys. **116**, 755 (2018).

[9] Y. Wang, B. C. Shepler, B. J. Braams, and J. M. Bowman, J. Chem. Phys. **131**, 054511 (2009).

[10] Y. Wang and J. M. Bowman, Phys. Chem. Chem. Phys. **18**, 24057 (2016).

[11] V. Babin, C. Leforestier, and F. Paesani, J. Chem. Theory Comput. **9**, 5395 (2013).

[12] C. Schran, J. Behler, and D. Marx, J. Chem. Theory Comput. **16**, 88 (2019).

[13] Y. Wang, X. Huang, B. C. Shepler, B. J. Braams, and J. M. Bowman, J. Chem. Phys. **134**, 094509 (2011).

[14] G. R. Medders, V. Babin, and F. Paesani, J. Chem. Theory Comput. **10**, 2906 (2014).

[15] S. K. Reddy, S. C. Straight, P. Bajaj, C. Huy Pham, M. Riera, D. R. Moberg, M. A. Morales, C. Knight, A. W. Götz, and F. Paesani, J. Chem. Phys. **145**, 194504 (2016).

[16] A. O. Caldeira and A. J. Leggett, Physica A **121**, 587 (1983).

[17] V. Molinero and E. B. Moore, J. Phys. Chem. B **113**, 4008 (2009).

[18] A. V. Marenich, C. J. Cramer, and D. G. Truhlar, J. Phys. Chem. B **113**, 6378 (2009).

[19] X. Sun and E. Geva, J. Chem. Phys. **144**, 044106 (2016).

[20] S. Mukamel, *Principles of nonlinear optical spectroscopy*, Vol. 6 (Oxford university press New York, 1995).

[21] Y. Tanimura and S. Mukamel, Phys. Rev. E **47**, 118 (1993).

[22] R. Conte and E. Pollak, J. Chem. Phys. **136**, 094101 (2012).

[23] F. Gottwald, S. D. Ivanov, and O. Kühn, J. Chem. Phys. **144**, 164102 (2016).

[24] M. Buchholz, F. Grossmann, and M. Ceotto, J. Chem. Phys. **148**, 114107 (2018).

[25] R. Martinazzo, B. Vacchini, K. H. Hughes, and I. Burghardt, J. Chem. Phys. **134**, 011101 (2011).

[26] F. Gottwald, S. D. Ivanov, and O. Kühn, J. Phys. Chem. Lett. **6**, 2722 (2015).

[27] W. H. Miller, J. Phys. Chem. A **105**, 2942 (2001).

[28] W. H. Miller and T. F. George, J. Chem. Phys. **56**, 5637 (1972).

[29] N. Makri and W. H. Miller, J. Chem. Phys. **89**, 2170 (1988).

[30] K. G. Kay, J. Chem. Phys. **100**, 4377 (1994).

[31] K. G. Kay, J. Chem. Phys. **100**, 4432 (1994).

[32] F. Grossmann and A. L. Xavier, Phys. Lett. A **243**, 243 (1998).

[33] R. Gelabert, X. Giménez, M. Thoss, H. Wang, and W. H. Miller, J. Phys. Chem. A **104**, 10321 (2000).

[34] E. Pollak, "The Semiclassical Initial Value Series Representation of the Quantum Propagator," in *Quantum Dynamics of Complex Molecular Systems* (Springer Berlin Heidelberg, Berlin, Heidelberg, 2007) pp. 259–271.

[35] S. V. Antipov, Z. Ye, and N. Ananth, J. Chem. Phys. **142**, 184102 (2015).

[36] M. S. Church, S. V. Antipov, and N. Ananth, J. Chem. Phys. **146**, 234104 (2017).

[37] M. S. Church, T. J. Hele, G. S. Ezra, and N. Ananth, J. Chem. Phys. **148**, 102326 (2018).

[38] M. S. Church and N. Ananth, J. Chem. Phys. **151**, 134109 (2019).

[39] T. Begusic, M. Cordova, and J. Vanicek, J. Chem. Phys. **150**, 154117 (2019).

[40] L. Bonnet, J. Chem. Phys. **153**, 174102 (2020).

[41] M. Werther, S. L. Choudhury, and F. Großmann, Int. Rev. Phys. Chem. **40**, 81 (2020).

[42] R. Conte and M. Ceotto, Quantum Chemistry and Dynamics of Excited States: Methods and Applications , 595 (2020).

[43] A. L. Kaledin and W. H. Miller, J. Chem. Phys. **118**, 7174 (2003).

[44] A. L. Kaledin and W. H. Miller, J. Chem. Phys. **119**, 3078 (2003).

[45] X. Ma, G. Di Liberto, R. Conte, W. L. Hase, and M. Ceotto, J. Chem. Phys. **149**, 164113 (2018).

[46] R. Conte, G. Botti, and M. Ceotto, Vib. Spectrosc. **106**, 103015 (2020).

[47] M. Buchholz, E. Fallacara, F. Gottwald, M. Ceotto, F. Grossmann, and S. D. Ivanov, Chem. Phys. **515**, 231 (2018).

[48] M. Ceotto, G. Di Liberto, and R. Conte, Phys. Rev. Lett. **119**, 010401 (2017).

[49] G. Bertaina, G. Di Liberto, and M. Ceotto, J. Chem. Phys. **151**, 114307 (2019).

[50] R. Conte, L. Parma, C. Aieta, A. Rognoni, and M. Ceotto, J. Chem. Phys. **151**, 214107 (2019).

[51] M. Micciarelli, F. Gabas, R. Conte, and M. Ceotto, J. Chem. Phys. **150**, 184113 (2019).

[52] M. Micciarelli, R. Conte, J. Suarez, and M. Ceotto, J. Chem. Phys. **149**, 064115 (2018).

[53] C. Aieta, M. Micciarelli, G. Bertaina, and M. Ceotto, Nat. Comm. **11**, 1 (2020).

[54] R. Conte, F. Gabas, G. Botti, Y. Zhuang, and M. Ceotto, J. Chem. Phys. **150**, 244118 (2019).

[55] M. Gandolfi, A. Rognoni, C. Aieta, R. Conte, and M. Ceotto, J. Chem. Phys. **153**, 204104 (2020).

[56] F. Gabas, G. Di Liberto, R. Conte, and M. Ceotto, Chem. Sci. **9**, 7894 (2018).

[57] F. Gabas, G. Di Liberto, and M. Ceotto, J. Chem. Phys. **150**, 224107 (2019).

[58] F. Gabas, R. Conte, and M. Ceotto, J. Chem. Theory Comput. **16**, 3476 (2020).

[59] M. Cazzaniga, M. Micciarelli, F. Moriggi, A. Mahmoud, F. Gabas, and M. Ceotto, J. Chem. Phys. **152**, 104104 (2020).

[60] A. Rognoni, R. Conte, and M. Ceotto, Chem. Sci. , Advance Article (2021).

[61] E. J. Heller, Acc. Chem. Res. **14**, 368 (1981).

[62] M. F. Herman and E. Kluk, Chem. Phys. **91**, 27 (1984).

[63] M. F. Herman, J. Chem. Phys. **85**, 2069 (1986).

[64] M. F. Herman, Annu. Rev. Phys. Chem. **45**, 83 (1994).

[65] K. G. Kay, Chem. Phys. **322**, 3 (2006).

[66] G. Di Liberto, R. Conte, and M. Ceotto, J. Chem. Phys. **148**, 014307 (2018).

[67] G. Di Liberto, R. Conte, and M. Ceotto, J. Chem. Phys. **148**, 104302 (2018).

[68] N. De Leon and E. J. Heller, J. Chem. Phys. **78**, 4005 (1983).

[69] M. Ceotto, S. Atahan, G. F. Tantardini, and A. Aspuru-Guzik, J. Chem. Phys. **130**, 234113 (2009).

[70] M. Ceotto, G. F. Tantardini, and A. Aspuru-Guzik, J. Chem. Phys. **135**, 214108 (2011).

[71] R. Conte, A. Aspuru-Guzik, and M. Ceotto, J. Phys. Chem. Lett. **4**, 3407 (2013).

[72] F. Gabas, R. Conte, and M. Ceotto, J. Chem. Theory Comput. **13**, 2378 (2017).

[73] M. L. Brewer, J. S. Hulme, and D. E. Manolopoulos, J. Chem. Phys. **106**, 4832 (1997).

[74] M. Tuckerman, *Statistical mechanics: theory and molecular simulation* (Oxford university press, 2010).

[75] V. Babin, G. R. Medders, and F. Paesani, J. Chem. Theory Comput. **10**, 1599 (2014).

[76] Y. Bouteiller and J. Perchard, Chem. Phys. **305**, 1 (2004).

[77] Y. Wang and J. M. Bowman, J. Chem. Phys. **134**, 154510 (2011).

[78] D. Ben-Amotz, J. Am. Chem. Soc. **141**, 10569 (2019).

[79] M. Buchholz, F. Grossmann, and M. Ceotto, J. Chem. Phys. **144**, 094102 (2016).

[80] H. Wang, M. Thoss, K. L. Sorge, R. Gelabert, X. Giménez, and W. H. Miller, The Journal of Chemical Physics **114**, 2562 (2001).

[81] M. Buchholz, F. Grossmann, and M. Ceotto, J. Chem. Phys. **147**, 164110 (2017).

[82] S. Dressler and W. Thiel, Chem. Phys. Lett. **273**, 71 (1997).

[83] O. Marsalek and T. E. Markland, J. Phys. Chem. Lett. **8**, 1545 (2017).